Detection of Changes in Land Cover and Land Surface Temperature Using Multi Temporal Landsat Data

Aye Aye Myint[1*] and Myat Myat Min[2]

[1]*Faculty of Computing, University of Computer Studies, Mandalay, Myanmar*
[2]*Faculty of Computer Science, University of Computer Studies, Mandalay, Myanmar*

ARTICLE INFO

Received: 18 Jul 2019
Received in revised: 18 Oct 2019
Accepted: 19 Nov 2019
Published online: 3 Jan 2020
DOI: 10.32526/ennrj.18.2.2020.14

Keywords:
Land cover/ Land surface temperature/ Change detection/ NDVI

*** Corresponding author:**
E-mail:
ayeayemyint@ucsm.edu.mm

ABSTRACT

Land cover changes and land surface temperature have rose in the tropical regions of Myanmar especially in the surrounding areas of Magway city due to the rapid growth of urban sprawl. This study investigated the patterns of land cover and the trend of land surface temperature in Magway city area between 1989 and 2017. For this purpose, Landsat 5 TM and Landsat 8 OLI were used and land surface temperatures (LST) were calculated through thermal data with Normalized Difference Vegetation Index (NDVI). After obtaining the land cover map by using maximum likelihood algorithm for each study period, the accuracy of this map was tested using 100 ground checkpoints in an error matrix. A statistical analysis of the results showed the increase of the built-up area by 11.7% and the decline of the vegetation area by 19.7% from 1989 to 2017. Moreover, land surface temperature has risen by 4 °C during this 28 years period. Therefore, this study is intended to help the Magway city development council plan effective land cover management in the future.

1. INTRODUCTION

Land cover (LC) is defined as the earth's surface attributes captured by vegetation, water, desert, and ice and it also includes structures created only by human activities such as mine exposure and settlement (Lambin et at., 2003). Land cover represents an important factor in the geographic analysis, from physical geography to environmental analysis and spatial planning approaches. This is a dynamic variable that reflects the interaction between socio-economic activity and local environmental changes and therefore needs to be updated frequently (Rujoiu and Mihai, 2016). LC information is essential for managing natural resources and monitoring of environmental changes (Bharath et al., 2013).

Moreover, land use/land cover (LULC) changes are considered as important tools for assessing global change at different space-time scales (Lambin, 1997). It is a widespread, accelerating, and important process which is driven by human behavior and at the same time results in changes that impact human livelihood (Agarwal et al., 2002). Land cover change refers to the conversion from one category of land cover to another and/or the modifications of conditions within a category (Meyer and Turner, 1992). These changes in the LULC system have important environmental consequences of impacts on soil and water, biodiversity and microclimate (Lambin et at., 2003).

Investigation of land cover change can be performed on a temporal scale, such as a decade to assess landscape change caused by anthropogenic activities on the land (Gibson and Power, 2000). More prominently, LULC change data are significant for environmental and climate change studies and developing considerate the multifaceted relations between anthropogenic actions and global temperature change (Jung et al., 2006; Gong et al., 2013). In addition, accurate and up-to-date information on land cover changes is needed to understand and assess the environmental impact of such changes (Lambin and Geist, 2008).

Knowledge of Land Surface Temperature (LST) and its temporal and spatial variations within a city environment is most important for the study of urban climate and human-environment interactions (Singh and Grover, 2014; Alavipanah et al., 2015). LST information at the regional and global scales can

Citation: Myint AA, Min MM. Detection of changes in land cover and land surface temperature using multi temporal Landsat data. Environ. Nat. Resour. J. 2020;18(2):146-155. DOI: 10.32526/ennrj.18.2.2020.14

be detected by sensor, since most of the energy in this spectral region is directly emitted from the surface (Sobrino, 2008). LST is determined by energy fluxes between the surface and the atmosphere (Voogt and Oke, 2003). LST can be obtained from thermal images depending on the number of bands using a single infrared channel or a split window method (Pu et al., 2006). LST is one of the main variables measured using remote sensing thermal bands of various sensors such as AVHRR, MODIS, Landsat-5TM, Landsat-7ETM+ and Landsat-8TIRS (Gebrekidan, 2016).

Many studies have investigated the relationship between LULC and LST using remote-sensing imagery on regional and global climate (Chen et al., 2017; Zhang et al., 2016). The relationship between LULC and LST is very important in land management and global climate change research. Therefore, LST measurements caused by changes in LULC can provide an indication of the expansion of heat distribution associated with LULC patterns and human-related changes. In addition, LST is sensitive to various land surface features and can be used to extract various land use/cover types information (Sinha et al., 2015).

Remote sensing data provides a way to understand the changes in spatio-temporal land cover related to basic physical properties in terms of surface radiance and emissivity data. Moreover, remote sensing technology in combination with geographic information system technology is an effective technique for the observation of land cover/use and land surface temperature changes (Orhan and Yakar, 2016).

This study investigated the spatial pattern of land cover changes and LST using remote sensing Landsat data within the period of 1989-2017. The objectives of this paper are (a) to generate the land cover classification map and LST map and (b) to estimate the pattern of land cover changes and the trend of LST in Magway city and its surrounding areas between 1989 and 2017.

2. METHODOLOGY

2.1 Study area

The study area is the capital city of Magway region, located at latitude 20°09′15″ North and longitude 094°56′43″ East with an area of about 146.6443 km^2 (Figure 1). It is situated in an arid region of the central part of Myanmar. The landscape of the region (Magway) is located on a plain with few valleys and is surrounded by Ayayarwaddy River in the west and Ying Creek in the south. The climate is a dry tropical type and is characterized by summer, rain and cold seasons. The summer season begins at the end of February and ends in mid-June. The rainy season is mostly from June to October. The remaining months are called the cold season. The mean annual rainfall is about 948.7 mm while average high temperature is 46.5 °C and low temperature is 8.2 °C (based on 2017 data from the Department of Meteorology and Hydrology, Magway). The temperature is very high and hottest in April and May.

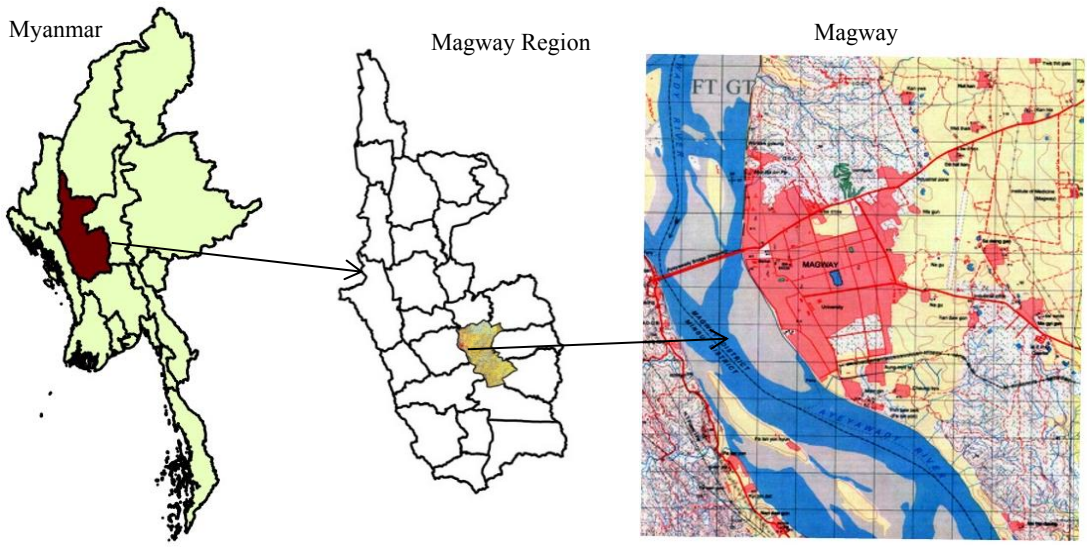

Figure 1. Location map of study area (Source – Myanmar Information Management Unit).

2.2 Landsat data

In this study, Landsat 5 TM for 1989, 2004 and Landsat 8 OLT/TIRS (path/row: 134/46) images were downloaded from US Geological Survey (http://earthexplorer.usgs.gov/). The obtained Landsat data (Level 1 Terrain Corrected (L1T) products were geometrically transformed to real world coordinates using UTM zone 46 North projections and WGS-84 datum. Meteorological data are obtained from Department of Meteorology and Hydrology, Magway. ArcGIS 10.1 and QGIS 3.0 are used for this entire study. The details of satellite data collected are shown in Table 1.

Table 1. Detail information of Landsat data

Satellite	Data acquisition	Sensors	Format
Landsat 5	21-04-1989	TM	GeoTIFF
Landsat 5	13-03-2004	TM	GeoTIFF
Landsat 8	02-04-2017	OLI/TIRS	GeoTIFF

2.3 Image preprocessing

Image preprocessing is required before image classification and extracts LST. The preprocessing step includes atmospheric correction, bands combination, and clipping the study area. Atmospheric correction is a necessary step to accurately extract quantitative information from the Landsat Data. These images were performed by Dark Object Subtraction method in QGIS 3.0. All the bands were used to produce a composite image for the purpose of land cover classification image analysis. Landsat images contain a very large area, so the study area is clipped by overlaying geo-referenced outline boundary of the study area using ArcGIS 10.1 software. The extraction of land surface temperature from thermal band images was employed in three study periods. The detailed methodology is shown in Figure 2.

2.4 Extract LST from thermal band

Thermal band 6 for Landsat 5 and band 10/11 for Landsat 8 were employed to calculate the LST from all the periods under the following phases. Meta data values are used for calculation of LST in the following Table 2.

At the first stage, the digital number was transformed into spectral radiance by using Equation 1 for Landsat 5 (Markham, 1986) and Equation 2 for Landsat 8 (Lee et al., 2012; Nichol and To, 2012).

$$L_\lambda = \left(\frac{L_{max} - L_{min}}{Qcal_{max}}\right) \times Qcal + L_{min} \quad (1)$$

$$L_\lambda = M_L \times Qcal + A_L \quad (2)$$

Where, L_λ is the spectral radiance in W/(m^2 sr µm). Qcal is the DN of each image, and $Qcal_{max}$ is the maximum DN (65535 for the 16-bit Landsat 8 and 255 for Landsat 5. L_{max} and L_{min} are the maximum and minimum top of atmospheric (TOA) radiances in W/(m^2 sr µm). M_L (0.0003342) and A_L (0.1) are band specific multiplicative and additive rescaling factors obtained from the image Meta data file.

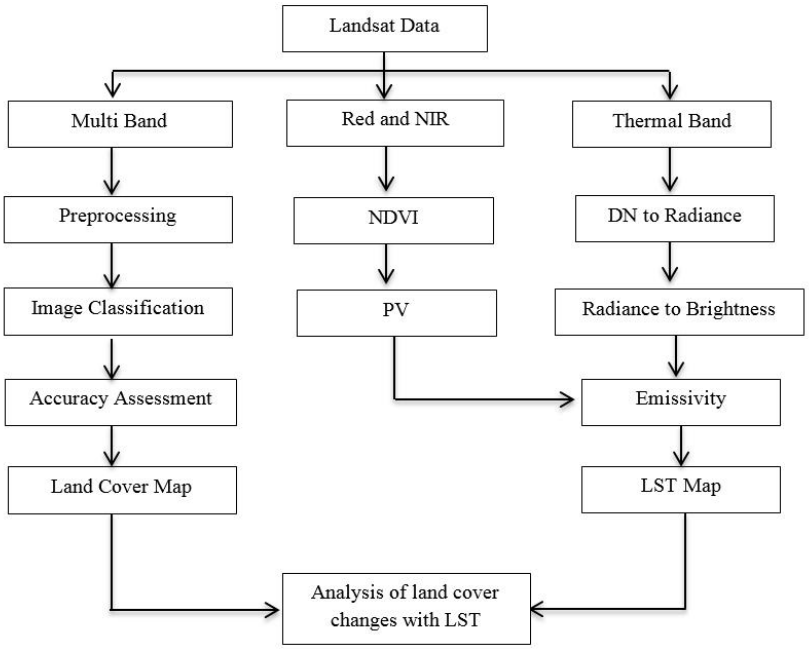

Figure 2. General work flow of methodology

At the second stage, the radiance was converted to brightness temperature in Celsius using Equation 3 (Chander and Markham, 2003).

$$T_b = \frac{K_2}{\ln\left(\frac{K_1}{L_\lambda} + 1\right)} - 273.15 \quad (3)$$

Where, T_b is the at-sensor brightness temperature in Celsius unit, L_λ is the spectral radiance, and K_1 and K_2 are calibration constants of Landsat 5/8 from Meta file.

Normalized Difference Vegetation Index (NDVI) was used for determination of land surface emissivity by using Equation 4 (Tucker, 1979).

$$NDVI = (NIR - Red) / (NIR + Red) \quad (4)$$

Where, NIR is near infrared band (band 4 for Landsat 5, band 5 for Landsat 8) and Red is red band (band 3 for Landsat 5, band 4 for Landsat 8).

Table 2. Values of parameters of Landsat images from Meta data

Variable	Description	Landsat 5	Landsat 8
L_{min}	Minimum values of radiance	1.238	-
L_{max}	Maximum values of radiance	15.303	-
$Qcal_{max}$	Maximum quantize calibration	255	65535
K_1	Thermal constant	607.76	774.8853
K_2	Thermal constant	1260.56	1321.0789

After the NDVI was computed; proportional vegetation (Pv) can be extracted by using Equation 5 with NDVI values (Sobrino et al., 2004).

$$P_v = [(NDVI - NDVI_{min}) / (NDVI_{max} - NDVI_{min})]^2 \quad (5)$$

Where, Pv is proportion of vegetation, $NDVI_{min}$ is minimum values of NDVI and $NDVI_{max}$ is maximum values of NDVI.

Land surface emissivity for each thermal band was computed based on proportion of vegetation using Equation 6 (Sobrino et al., 2004).

$$\varepsilon = 0.004 \times Pv + 0.986 \quad (6)$$

Where, ε is land surface emissivity, Pv is proportion of vegetation.

At the final stage, land surface temperatures were estimated from brightness temperatures (emissivity correction) by using Equation 7 (Artis and Carnahan, 1982).

$$LST = \frac{T_b}{\left[1 + \left\{\left(\frac{T_b}{\rho} \times \lambda\right)\right\} \times \ln \varepsilon\right]} \quad (7)$$

Where, LST is the land surface temperature, λ is the wavelength of emitted radiance in meters (λ=11.5 µm), ε is land surface emissivity, T_b is the brightness temperature in Celsius and $\rho = h \times c/\sigma = 1.438 \times 10^{-2}$ mK (σ=Boltzmann constant $=1.38 \times 10^{-23}$ J/K, h=Planck's constant$=6.626 \times 10^{-34}$ Js, c=velocity of light$= 2.998 \times 10^{8}$ m/s).

2.5 Classification of land cover

In this research, the supervised classification (maximum likelihood algorithm) was employed mapping the land cover of the study area. For this classification, the images of study area were categorized into five classes including water body, sand bar, built up, agricultural and sparse vegetation land as shown in Table 3. Training data are collected from the field survey and use of Google Earth. Maximum Likelihood algorithm classifies a pixel taking into account the variance and the covariance of the spectral response pattern of each category. A probability density function is created for each spectral category used to classify unknown pixels by calculating the probability that the pixel belongs to each class. Pixels are assigned to classes with a higher probability. It is the greatest classification method when accurate training data is provided (Schowengerdt, 2006; Lillesand et al., 2015).

Table 3. Descriptions of land cover class

Class	Description
Water body	River, lake
Sand bar	Sandy land, bare land, wet land
Built up	Urban and rural land
Agricultural	Peanut, bean, sesame and dry farm land
Vegetation	Sparse vegetation, grass or tropical savannah , shrubs, open tropical land

2.5.1 Accuracy assessment of land cover map

In this study, 100 random points were done by using the stratified random sampling techniques to get accurate assessment of each classified image. Random points were a minimum distance of 10 m apart to avoid selecting the same pixel. These points are exported into a ".kml" file for viewing on Google Earth. Each of these points is examined to identify whether it belongs to "water" or "other" class and so on. This process is done for all of these points on the classified images from 1989 to 2017. The comparison of reference data (ground check points) and classification results was carried out statistically using error matrix. The following formulas are measured for each classification images (Lillesand et al., 2015).

$$\text{User Accuracy} = \frac{\text{Total number of correctly classified samples in each category}}{\text{Total number of classified samples in that category (row total)}} \times 100 \quad (8)$$

$$\text{Producer Accuracy} = \frac{\text{Total number of correctly classified samples in each category}}{\text{Total number of classified samples in that category (col total)}} \times 100 \quad (9)$$

$$\text{Overall Accuracy} = \frac{\text{Total number of correctly classified samples}}{\text{Total number of reffernce samples}} \times 100 \quad (10)$$

$$\text{Kappa Coefficient} = \frac{[(\text{Total sum correct}) - \text{sum of all (col total} \times \text{row total)}]}{[(\text{Total sum correct})^2 - \text{sum of all (col total} \times \text{row total)}]} \quad (11)$$

3. RESULTS AND DISCUSSION

3.1 Land cover classification

Supervised classification of multiple Landsat images is an effective tool to quantify current LU / LC and detect in environmental changes (Cheruto et al., 2016). In this study, the classification images generated the five major LC features of Magway city and its surrounding area for 1989 and 2017 as shown in Figure 3. The classified images were assessed for accuracy based on 100 random reference points for each class over the study period. Accuracy assessment is an important parameter for urban growth and LST (Wang et al., 2018). Table 4 shows the overall accuracy and Kappa coefficient of 1989, 2004, and 2017 is above 86% and 0.83 of the classified images. Areas of spatial and temporal LC were calculated between 1989 and 2017.

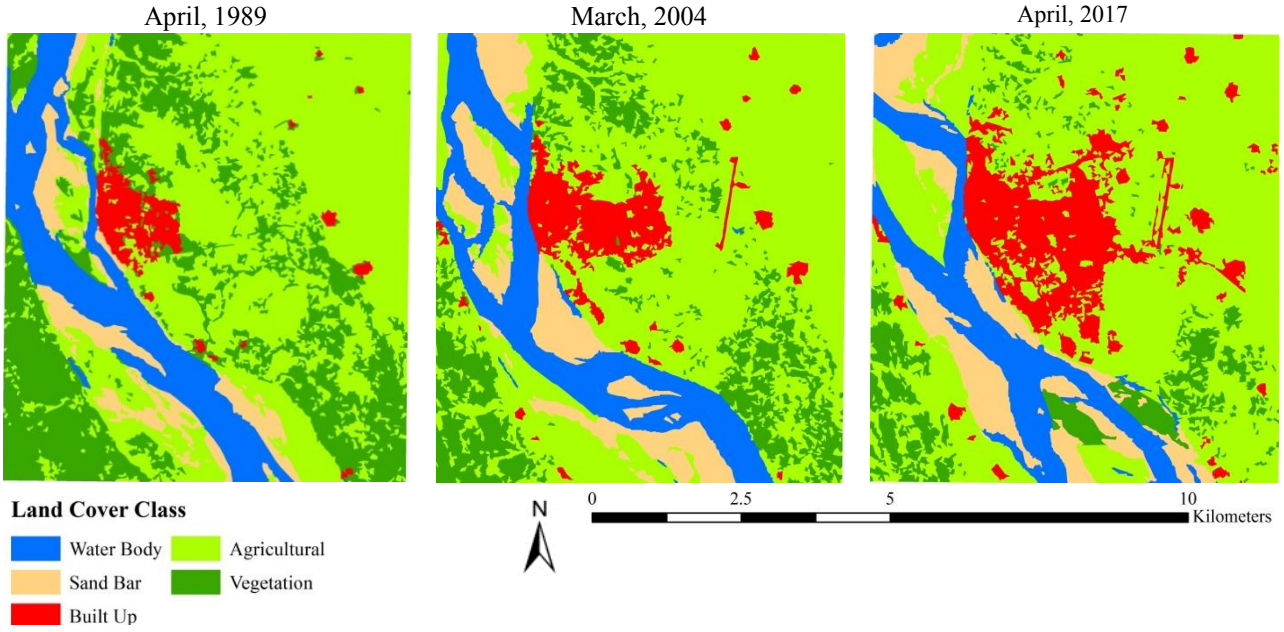

Figure 3. Land covers maps for 1989, 2004 and 2017

Table 4. Accuracy assessment of land cover from 1989 to 2017

Year	User accuracy (%)					Producer accuracy (%)					Overall	K
	Water body	Sand bar	Built up	Agriculture	Vegetation	Water body	Sand bar	Built up	Agriculture	Vegetation	Accuracy	Coefficient
1989	90	90	85	90	75	100	90	100	66.7	83.3	86%	0.83
2004	80	90	100	80	90	88.9	78.3	100	88.9	85.7	88%	0.85
2017	100	95	90	80	95	95.2	100	94.7	94.1	79.2	92%	0.9

The results of LC changes in the study area showed that built up area has dramatically expanded to occupy agriculture and vegetation areas from 4.8 km^2 in 1989, to 9.7 km^2 in 2004 and 21.9 km^2 in 2017. The area of water body slightly increased from 18.3 km^2 in 1989 to 19.9 km^2 in 2004 and decreased to 15.98 km^2 in 2017. Sand bar increased from 9.9 km^2 in 1989 to 14.6 km^2 in 2004 and slightly decreased to 12.4 km^2 in 2017. Vegetation has also decreased from 39.1 km^2 in 1989 to 21.2 km^2 in 2004 and slightly decreased to 10.4 km^2 in 2017. Agriculture increased from 73.9 km^2 in 1989 to 81.3 km^2 in 2004, and 85.95 km^2 in 2017 (Table 5).

According to the statistics results, the urbanization is rapidly increasing where most agricultural land is transformed into built up land. Vegetation land has been converted into agricultural and also into built up land. Water body has been transformed into sand bar and agricultural land. Sand bar has been transformed into water body and agricultural land during the study periods. These changes of temporal trend in the study area, mainly focused on five types, are due to the population increase and their needs for adequate food supply, secure housing and socio-economic activities. With the population increase, the built up area and agricultural area have increased from year to year.

In summary, all land cover classes except water area and sand bar showed high change rate between the study areas. The water body and sand bar have fluctuating changes over the period. Figure 4 shows the gain or loss in land cover type.

Table 5. Statistics of land cover from 1989 to 2017

Land cover	1989		2004		2017		1989-2004	2004-2017
Type	Acres	%	Acres	%	Acres	%	Change of area	Change of area
Water body	18.33	12.6	19.90	13.6	15.98	10.9	1.57	-3.92
Sand bar	9.95	6.8	14.60	10	12.37	8.4	4.65	-2.22
Built up	4.78	3.3	9.65	6.6	21.91	14.9	4.87	12.26
Agricultural	73.85	50.6	81.31	55.4	85.95	58.6	7.45	4.65
Vegetation	39.12	26.9	21.20	14.5	10.41	7.1	-17.93	-10.79

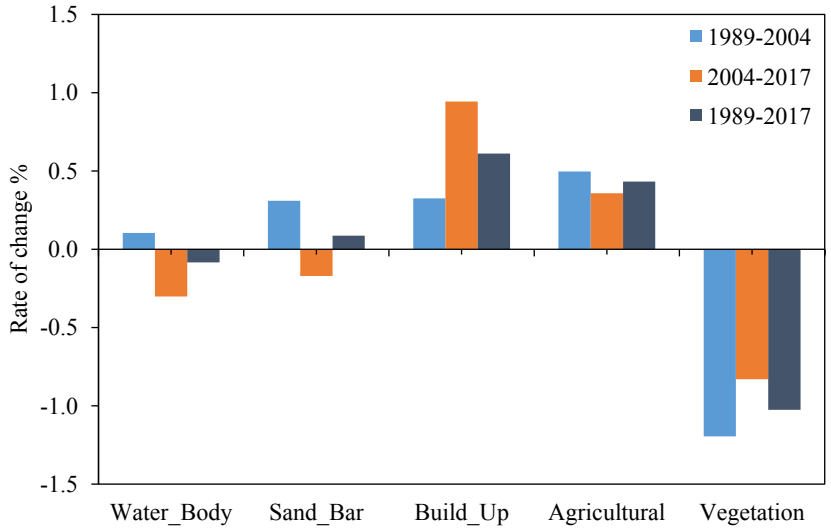

Figure 4. Change trends of land cover between 1989 and 2017

Land use/cover changes are complex and at the same time interrelated such that the expansion of one land cover type occurs at the expense of other land cover classes (Shiferaw and Singh, 2011). Cansong and Lede (2014) proposed the expansion of agricultural land is at the expense of lands with natural vegetation cover. The results of this study are consistent with the results of other studies. In our study results, the expansion of built up and agricultural land had previously been vegetation land. Agriculture is the most important sector of Myanmar's economy.

3.2 Land surface temperature

The LST map is extracted by using a single channel method from the thermal infrared band of Landsat data for 1989, 2004 and 2017 shown in Figure 5. The results of LST has been presented in Table 6, the surface temperatures were recorded in the range of 24-39 °C in 1989, the temperature ranges from 23-38 °C in 2004 and ranges from 26-43 °C in 2017, respectively. Therefore, temperature change significantly increased in 2017, the highest temperature recorded was 43 °C and lowest temperature was 26 °C. The most important indicator would be the maximum temperature. The maximum temperature change was about 1 °C decrease between 1989 and 2004 and increase of 5 °C from 2004 to 2017.

An assessment of these areas was done using a ground validation technique in order to get a better understanding of these changes. It was discovered that LST has decreased by nearly 1 °C which is probably due to the fact that the water body areas have increased by 1.6 km^2 during 1989 and 2004. The LST of study area has increased by 5 °C was growth of human activities such as industrial, residential and expanded agricultural are established from 2004 to 2017. When increasing development of built up areas, expanded agricultural and decreasing vegetation can be influenced to LST increase by 5 °C from 2004 to 2017. After 28 years, the maximum temperature increased by 4 °C which is a pointer to the change in the spatial pattern of the LST in study area. Moreover, comparison between temperatures at the Meteorological station (Magway) and surface temperature of LST map showed the estimated LST value was less than 3 °C.

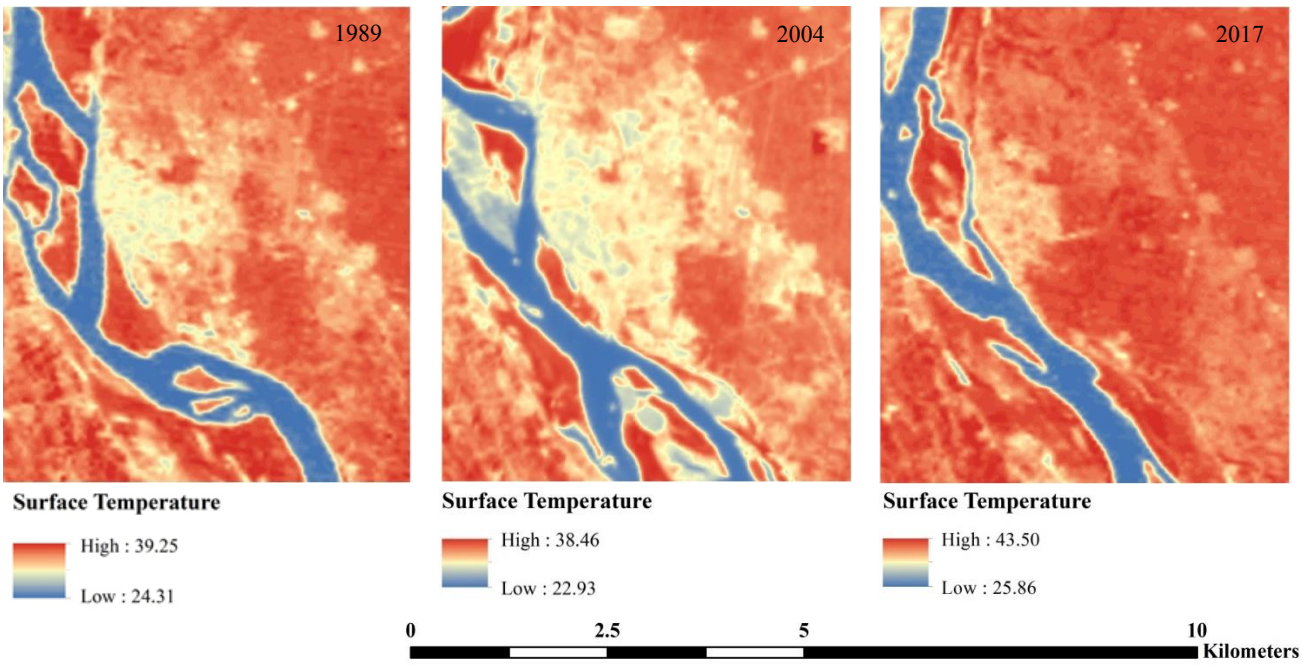

Figure 5. Land surface temperature maps extract from Landsat images for 1989, 2004, 2017

Table 6. Statistics of land surface temperature for 1989, 2004 and 2017

Year	Min	Max	Mean	Std Dev	Coefficient variation
1989	24.31	39.25	35.07	3.61	0.10
2004	22.93	38.46	33.02	3.64	0.11
2017	25.86	43.50	36.35	3.91	0.10

As shown in Figure 6, the mean surface temperature values fluctuate between 1989 and 2017. It can be concluded that the LST trend in the study area increases between the years 2004 and 2017. However, this trend has changed showing higher values since 2004. Despite the slight decrease in 2004, the overall trend of surface temperature shows an increasing trend.

Land cover has a significant impact on surface temperature. Conversion of land cover types increases the effect of surface temperature and greatly influences the number and distribution of hot spots (Tran et al., 2017).

From the analysis of this study, the relationship between LC and LST observed that the mean LST of sand bar was higher than other LC classes over the study periods. The mean LST of built up area was 33.48 °C on 1989, whereas the built up mean LST was slightly lower at 31.06 °C on 2004 and it was slightly higher at 34.86 °C on 2017 (Table 7). The agricultural land had a higher mean LST (Figure 7) due to the fact that the agricultural pixels were a mix of harvested area and unplanted bare soil. Zhang et al. (2013) revealed that agricultural area was characterized by the highest LST which is probably due to the fact that these areas consisted of mainly unplanted bare soil, as bare surfaces are usually characterized by higher LST than planted crop covers. Therefore, the agriculture trend is to shift from actively growing crops. Like agricultural, vegetation had the higher mean LST because the vegetation pixels were a mixture of the spare vegetation, tropical savannah and dried plants.

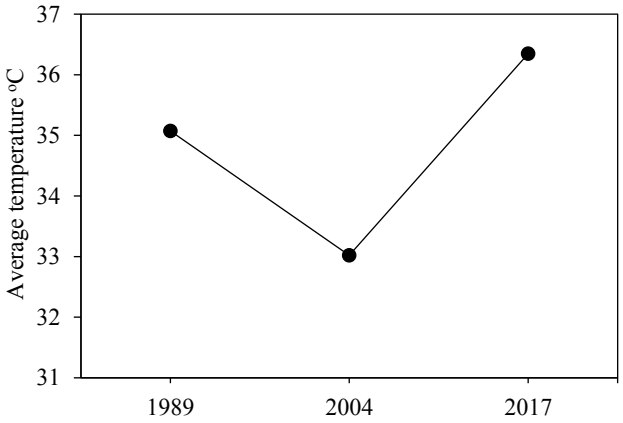

Figure 6. Mean surface temperature of the study area in 1989 - 2017

Table 7. Mean and standard deviation (STD) of LST in each LC class for 1989, 2004, 2017

Year	LST	Water body	Sand bar	Built up	Agricultural	Vegetation
1989	Mean	26.41	36.47	33.48	36.68	35.93
	STD	2.07	1.93	0.79	1.01	1.5
2004	Mean	25.19	35.38	31.06	34.31	34.67
	STD	2.21	1.77	1.00	1.66	1.22
2017	Mean	27.84	39.06	34.86	37.62	37.59
	STD	2.2	2.94	1.05	2.39	2.37

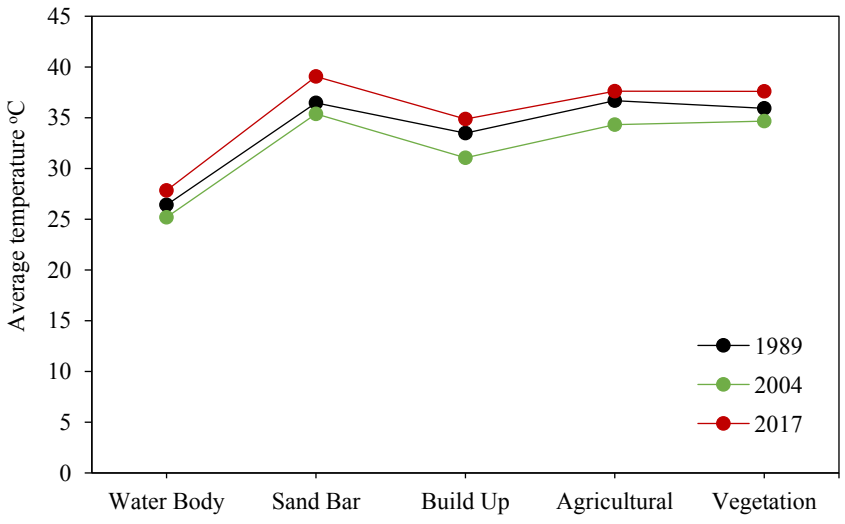

Figure 7. Mean surface temperature in each LC category for three dates

The main reason is probably due to differences in general weather conditions at the time of image acquisition and LC changes (growth in built up and agricultural, degradation of healthy vegetation) during the study dates. However, the average LST of overall area for the study observation years has increase rate 0.94 °C to 2.59 °C, it signifies effect on local and global warming; this is closely related with the rapidly expanding urban and agricultural.

4. CONCLUSION

This study has presented spatio-temporal changes of land cover and LST over a 28-year period in Magway city and its surrounding areas. Landsat satellite data were used to extract land cover information with five major categories, and LST was measured from the thermal band and then analysed for the changes and relationship of LST and LC. The land cover change was observed as the expansion of built up area due to exponential growth of population, rapidly growing infrastructure and poor land use planning. Agricultural areas were extended for higher production and to earn more income. On the other hand, vegetation area has experienced high conversion rate and decreased by an amount of -28.7 km^2 from 1989 to 2017. The analyzed trend of temperature change indicates maximum temperature change is from 39-43 °C between 1989 and 2017. Similarly, the minimum temperature change ranges from 24-26 °C between these periods. This research point out that land cover change is an important cause for rising land surface temperature. The combination of remote sensing and GIS technologies produces powerful analysis and a monitoring system for future management and planning of landscape.

REFERENCES

Agarwal C, Green GM, Grove JM, Evans TP, Schweik CM. A Review and Assessment of Land-use Change Models: Dynamics of Space, Time, and Human Choice. Newton Square, PA: USDA Forest Service; 2002.

Alavipanah S, Wegmann M, Qureshi S, Weng Q, Koellner T. The role of vegetation in mitigating urban land surface temperatures: A case study of Munich, Germany during the warm season. Sustainability 2015;7(4):4689-706.

Artis DA, Carnahan WH. Survey of emissivity variability in thermography of urban areas. Remote Sensing of Environment 1982;12(4):313-29.

Bharath S, Rajan KS, Ramachandra TV. Land surface temperature responses to land use land cover dynamics. Geoinformatics Geostatistics: An Overview. 2013;1(4):1-10.

Cansong L, Lede N. Analysis on spatial-temporal distribution patten and change characteristics of land cover in Burma based on high-resolution remote sensing image and GIS technology. Proceedings of the 7th International Conference on Intelligent Computation Technology and Automation; 2014 Oct 25-26; Changsha: China; 2014.

Chander G, Markham B. Revised Landsat-5 TM radiometric calibration procedures and postcalibration dynamic ranges. IEEE Transactions on Geoscience and Remote Sensing 2003; 41(11):2674-7.

Chen YC, Chiu HW, Su YF, Wu YC, Cheng KS. Does urbanization increase diurnal land surface temperature variation? Evidence and implications. Landscape and Urban Planning 2017;157:247-58.

Cheruto MC, Kauti MK, Kisangau DP, Kariuki PC. Assessment of land use and land cover change using GIS and remote sensing techniques: A case study of Makueni County, Kenya. Journal of Remote Sensing and GIS 2016;5:1-6.

Gebrekidan, Werku. Modeling land surface temperature from satellite data, the case of Addis Ababa. Proceedings of the United Nations Conference Centre Addis Ababa; 2016 Sep 23-24; Africa Hall, Addis Ababa: Ethiopia; 2016.

Gibson PJ, Power CH. Introductory Remote Sensing: Digital Image Processing and Applications. London, United Kingdom: Routledge; 2000.

Gong P, Wang J, Yu L, Zhao Y, Zhao Y, Liang L, Niu Z, Huang X, Fu H, Liu S, Li C. Finer resolution observation and monitoring of global land cover: First mapping results with Landsat TM and ETM+ data. International Journal of Remote Sensing 2013;34(7):2607-54.

Jiménez-Muñoz JC, Sobrino JA. Split-window coefficients for land surface temperature retrieval from low-resolution thermal infrared sensors. IEEE Geoscience and Remote Sensing Letters 2008;5(4):806-9.

Jung M, Henkel K, Herold M, Churkina G. Exploiting synergies of global land cover products for carbon cycle modeling. Remote Sensing of Environment 2006;101(4):534-53.

Lambin EF, Geist HJ, Lepers E. Dynamics of land-use and land-cover change in tropical regions. Annual Review of Environment and Resources 2003;28(1):205-41.

Lambin EF, Geist HJ. Land-Use and Land-Cover Change: Local Processes and Global Impacts. Heidelberg, Germany: Springer; 2008.

Lambin EF. Modelling and monitoring land-cover change processes in tropical regions. Progress in Physical Geography 1997;21(3):375-93.

Lee TW, Lee JY, Wang ZH. Scaling of the urban heat island intensity using time-dependent energy balance. Urban Climate 2012;2:16-24.

Lillesand T, Kiefer RW, Chipman J. Remote Sensing and Image Interpretation. Hoboken, New Jersey, USA: John Wiley and Sons; 2015.

Markham BL. Landsat MSS and TM post-calibration dynamic ranges, exoatmospheric reflectances and at-satellite temperatures. Landsat Technical Notes 1986;1:3-8.

Meyer WB, Turner BL. Human population growth and global land-use/cover change. Annual Review of Ecology and Systematics 1992;23(1):39-61.

Nichol JE, To PH. Temporal characteristics of thermal satellite images for urban heat stress and heat island mapping. ISPRS Journal of Photogrammetry and Remote Sensing 2012;74(1):153-62.

Orhan O, Yakar M. Investigating land surface temperature changes using Landsat data in Konya, Turkey. International Archives of Photogrammetry, Remote Sensing and Spatial Information Sciences 2016;41:285-89.

Pu R, Gong P, Michishita R, Sasagawa T. Assessment of multi-resolution and multi-sensor data for urban surface temperature retrieval. Remote Sensing of Environment 2006;104(2):211-25.

Rujoiu-Mare MR, Mihai BA. Mapping land cover using remote sensing data and GIS techniques: A case study of Prahova Subcarpathians. Procedia Environmental Sciences 2016; 32:244-55.

Schowengerdt RA. Remote sensing: Models and methods for image processing. California, USA: Elsevier; 2006.

Shiferaw A, Singh KL. Evaluating the land use and land cover dynamics in Borena Woreda South Wollo Highlands, Ethiopia. Ethiopian Journal of Business and Economics (The) 2011;(2)1:69-104.

Singh R, Grover A, Zhan J. Inter-seasonal variations of surface temperature in the urbanized environment of Delhi using Landsat thermal data. Energies 2014;7(3):1811-28.

Sinha S, Sharma LK, Nathawat MS. Improved land-use/land-cover classification of semi-arid deciduous forest landscape using thermal remote sensing. Egyptian Journal of Remote Sensing and Space Science 2015;18(2):217-33.

Sobrino JA, Jimenez-Munoz JC, Paolini L. Land surface temperature retrieval from LANDSAT TM 5. Remote Sensing of environment 2004;90(4):434-40.

Tran DX, Pla F, Latorre-Carmona P, Myint SW, Caetano M, Kieu HV. Characterizing the relationship between land use land cover change and land surface temperature. ISPRS Journal of Photogrammetry and Remote Sensing 2017;124:119-32

Tucker CJ. Red and photographic infrared linear combinations for monitoring vegetation. Remote Sensing of Environment 1979;8(2):127-50.

Voogt JA, Oke TR. Thermal remote sensing of urban climates. Remote Sensing of Environment 2003;86(3):370-84.

Wang S, Ma Q, Ding H, Liang H. Detection of urban expansion and land surface temperature change using multi-temporal Landsat images. Resources, Conservation and Recycling 2018;128:526-34.

Zhang F, Tiyip T, Kung H, Johnson VC, Maimaitiyiming M, Zhou M, Wang J. Dynamics of land surface temperature (LST) in response to land use and land cover (LULC) changes in the Weigan and Kuqa river oasis, Xinjiang, China. Arabian Journal of Geosciences 2016;9(7):499.

Zhang Y, Odeh IO, Ramadan E. Assessment of land surface temperature in relation to landscape metrics and fractional vegetation cover in an urban/peri-urban region using Landsat data. International Journal of Remote Sensing 2013;34(1): 168-89.